Available online at www.sciencedirect.com

ScienceDirect

IFAC PapersOnline CONFERENCE PAPER ARCHIVE

IFAC PapersOnLine 51-3 (2018) 62–67

A port-Hamiltonian Fluid-Structure Interaction Model for the Vocal folds ⋆

Luis A. Mora * **Juan I. Yuz** * **Hector Ramirez** ** **Yann Le Gorrec** **

* *Department of Electronic Engineering, Universidad Técnica Federico Santa María, Valparaíso, Chile (e-mail: luis.moraa@sansano.usm.cl, juan.yuz@usm.cl).*

** *FEMTO-ST, UMR CNRS 6174, département AS2M, Université de Bourgogne Franche-Comté, Besançon, France (e-mail:hector.ramirez@femto-st.fr, legorrec@femto-st.fr)*

Abstract: Fluid-structure interaction models are of special interest for studying the energy transfer between the moving fluid and the mechanical structure in contact. The vocal folds are an example of a fluid-structure system, where the mechanical structure is usually modeled as a mass-spring-damper system. In particular, the estimation of the collision forces of the vocal folds is of high interest in the diagnosis of phonotraumatic voice pathologies. In this context, the port-Hamiltonian modeling framework focuses on the energy flux in the model and the interacting forces. In this paper, we develop a port-Hamiltonian fluid-structure interaction model based on the interconnection methodology proposed by Lopes and Hélie (2016).

Keywords: Dynamic modeling, port-Hamiltonian model, fluid-structure interaction, vocal folds.

1. INTRODUCTION

Fluid-structure interaction (FSI) appears in different fields of engineering. Such as, the modeling of flexible wings (Hamamoto et al., 2005) and liquid sloshing in moving containers (Cardoso-Ribeiro et al., 2017) to cite some examples. An accurate modeling of these systems involving FSI is of particular interest when simulation or control of energy flows between the fluid and the mechanical structure in contact are considered.

In Lopes and Hélie (2016) an energy model of a jet interacting with a brass player lip is proposed. The behavior of the lip is represented by one contact mass with a spring-damper system. For the jet a two-dimensional airflow is used, whose behavior is given by the solution of the continuity equation (Bird et al., 2014) constrained to boundary conditions. The interconnection between the fluid and the structure is given by the definition of a vertical pseudo-momentum. This pseudo-momentum considers the mass and vertical airflow momenta, assuming that the vertical air velocity in the contact surface and mass velocity are the same.

The human vocal folds can be studied as a particular case of a FSI system. The vocal folds behavior has been modeled as interconnected mass-spring-damper systems, for example, in Story and Titze (1995). In this model the movement of the vocal folds is linked to displacements of each mass, where the system inputs are the forces applied to each mass. These forces are induced by the sub-glottal and supra-glottal pressures. In Encina et al. (2015) a port-Hamiltonian (PH) version of the Story and Titze (1995) model was proposed, however, considering the mechanical part only.

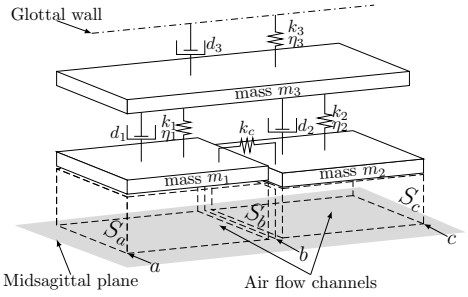

Fig. 1. Hemi-larynx glottis model

In this paper, we propose a PH model for the interaction between the vocal folds and the glottis airflow. We assume a symmetric behavior of the vocal folds.Then only a hemi-larynx is considered, as shown in Figure 1. The vocal fold is represented by the mass-spring-damper system. As consequence, the transverse air velocity is assumed to vanish on midsagittal plane and the glottal closure arises when the contact masses reach this plane. We use the procedure proposed by Lopes and Hélie (2016) to obtain an analytical description of the air velocities in the glottal channel and the interconnection between the fluid and structure PH models. In the fluid model we consider the boundary conditions given by the different configurations of the contact masses, obtaining the air velocity solution that converges to the particular solution corresponding to each glottis configuration.

⋆ This work was supported by CONICYT-PFCHA/2017-21170472, and AC3E CONICYT-Basal Project FB-0008.

10.1016/j.ifacol.2018.06.016

Table 1. Variables used for the fluid model

Label	Definition	Description
A_1	$2L\ell_0$	Area of the contact surface S_1 of mass m_1
A_2	$2L\ell_0$	Area of the contact surface S_2 of mass m_2
π_{ϑ_i}	$m_{\vartheta_i}\theta_i$	Longitudinal momentum of airflow on Ω_i
π_{φ_i}	$m_{\varphi_i}\psi_i$	Transverse momentum of airflow on Ω_i
C_{ϑ_i}	$1/m_{\vartheta_i}$	Inverse of axial effective mass on Ω_i
C_{φ_i}	$1/m_{\varphi_i}$	Inverse of transverse effective mass on Ω_i
$\langle f\rangle_X$	$\frac{\int_X f dX}{\int_X dX}$	Average of f over X
F_1	$A_1\langle p\rangle_{S_1}$	Force applied over mass m_1
F_2	$A_2\langle p\rangle_{S_2}$	Force applied over mass m_2
ϑ_{ix}	$\langle\vartheta_i\rangle_{S_x}$	Mean axial velocity in surface S_x

2. AIRFLOW MODEL

To model the airflow we consider four possible cases that change the fluid dynamics in the glottal tract (Figure 2). In Cases 1 and 2 the airflow channel is closed by the collision of one mass. In Cases 3 and 4, the airflow interacts with the two masses.

Assumption 1. To obtain the airflow dynamics in the glottis, we consider an incompressible and irrotational flow, i.e, the continuity equation of the fluid is reduced to

$$\nabla\cdot\mathbf{v}_i = 0 \tag{1}$$

where $\mathbf{v}_i = [\vartheta_i\ \varphi_i]^T$ is the air velocity vector below mass $m_i, i\in\{1,2\}$, ϑ_i and φ_i are the axial and transverse air velocities in Ω_i respectively [1], Ω_i is the volume of the channel section below mass m_i and L is the length of mass m_i in the sagittal axis.

In the next sections, we develop the PH model for each case. We define four zones of the glottal channel, as shown in Figure 2. S_k represent the transversal surfaces of each zones in corresponding points a, b and c. Finally, the variables and operators used in the fluid model are summarized in Table 1.

2.1 Model for Case 1 and Case 2

In Case 1 the right hand side of the channel is closed, as shown in Figure 2. Following the methodology of Lopes and Hélie (2016), we consider the point $x=0$ as the axial midpoint in Ω_1, the boundary conditions are given by $\vartheta_1|_{x=\ell_0}=0$, $\varphi_1|_{y=h_1}=\dot{h}_1=\psi_1$ and $\varphi_1|_{y=0}=0$, where ψ_1 is the vertical velocity of mass m_1. The solution of (1) with these boundary conditions, is given by

$$\vartheta_1(x,t)=\frac{\psi_1}{h_1}(\ell_0-x),\qquad \varphi_1(y,t)=\frac{\psi_1}{h_1}y \tag{2}$$

The kinetic energy in Ω_1 is given by

$$\mathcal{E}_1=\int_{\Omega_1}\frac{\rho}{2}|\mathbf{v}_1|^2 d\Omega_1=\frac{1}{2}m_{\varphi_1}\psi_1^2 \tag{3}$$

where $m_{\varphi_1}=\rho\frac{A_1}{3}\frac{h_1^2+4\ell_0^2}{h_1}$ is the effective mass of φ_1. Using π_{φ_1}, $\mathcal{E}_1$ and its time derivative are given by

$$\mathcal{E}_1=\frac{1}{2}C_{\varphi_1}\pi_{\varphi_1}^2 \tag{4}$$

$$\dot{\mathcal{E}}_1=\psi_1\left(\frac{\partial\mathcal{E}_1}{\partial h_1}+\dot{\pi}_{\varphi_1}\right) \tag{5}$$

where $\frac{\partial\mathcal{E}_1}{\partial\pi_{\varphi_1}}=C_{\varphi_1}\pi_{\varphi_1}=\psi_1$.

Considering Assumption 1 and neglecting the gravitational force and turbulence, the power balance for a fluid is given by

$$\nabla\cdot\left(\frac{\rho}{2}|\mathbf{v}_i|^2\mathbf{v}_i\right)+\nabla\cdot(p\mathbf{v}_i)=-\frac{\partial}{\partial t}\left(\frac{\rho}{2}|\mathbf{v}_i|^2\right) \tag{6}$$

where p is the static pressure on Ω_i. Integrating on Ω_1 and using the Gauss divergence theorem and Leibniz integral rule (Bird et al., 2014) we obtain

$$\dot{\mathcal{E}}_1=\int_{S_{a2}}\left(p+\frac{\rho}{2}|\mathbf{v}_1|^2\right)\vartheta_1 dS_{a2}-\int_{S_1}p\varphi_1 dS_1 \tag{7}$$

Considering the static pressure in a as $P_a=\langle p\rangle_{S_{a2}}$, $A_a\langle\vartheta_1\rangle_{S_{a2}}\left\langle\frac{\rho}{2}|\mathbf{v}_1|^2\right\rangle_{S_{a2}}\approx-\mathcal{D}_a$ represents the power dissipation through S_{a2} (neglecting the transverse velocity), and using F_1 and $A_a=Lh_1$ we can rewrite (7) as

$$\dot{\mathcal{E}}_1=A_a\vartheta_{1a2}P_a-\mathcal{D}_a-\psi_1F_1 \tag{8}$$

As a consequence of Assumption 1, the dissipation is due to jet flow mixing with downstream air and turbulence when the gas expends through the transversal surfaces in points a and c. According to Hager (2010), the energy losses are closely linked to the dynamic pressure. In general, we define the power dissipation through a surface S_k by

$$\mathcal{D}_k=sign\left(\langle\vartheta_i\rangle_{S_k}\right)\kappa_d A_k\langle\vartheta_i\rangle_{S_k}\left\langle\frac{\rho}{2}\vartheta_i^2\right\rangle_{S_k}s_k \tag{9}$$

where A_k is the area of S_k, κ_d is a dissipation factor and s_k is equal to 1 when the airflow flows out of the studied volume through the surface S_k and 0 in otherwise.

Given that ϑ_1 is constant in S_{a2}, the dissipation $\mathcal{D}_a$ in Case 1 is given by

$$\mathcal{D}_a=-\kappa_d A_a\frac{\rho}{2}\vartheta_{1a2}^3 s_{a2} \tag{10}$$

where $s_{a2}=1$ when $\vartheta_{1a2}<0$ and $s_{a2}=0$ otherwise. Using $\frac{\partial\mathcal{E}_1}{\partial\pi_{\varphi_1}}$, $\vartheta_1|_{x=-\ell_0}$, A_a and A_1, we can rewrite (10) as

$$\mathcal{D}_a=\vartheta_{1a2}g_1\frac{\partial\mathcal{E}_1}{\partial\pi_{\varphi_1}}s_{a2} \tag{11}$$

where $g_1=-\kappa_d A_1\frac{\rho}{2}\vartheta_{1a2}$.

Using (11) and $\vartheta_1|_{x=-\ell_0}$ we can rewrite (8) as

$$\dot{\mathcal{E}}_1=\psi_1\left(A_1P_a-\frac{2\ell_0}{h_1}g_1\frac{\partial\mathcal{E}_1}{\partial\pi_{\varphi_1}}s_a-F_1\right) \tag{12}$$

Matching (12) and (5), and defining $x_1=[h_1\ \pi_{\varphi_1}]^T$ we obtain the following PH model

$$\dot{x}_1=\begin{bmatrix}0 & 1\\ -1 & -2\frac{\ell_0}{h_1}g_1s_a\end{bmatrix}\nabla\mathcal{E}_1+\begin{bmatrix}0 & 0\\ -1 & A_1\end{bmatrix}\begin{bmatrix}F_1\\ P_a\end{bmatrix} \tag{13}$$

$$y_1=\begin{bmatrix}0 & -1\\ 0 & -A_1\end{bmatrix}\nabla\mathcal{E}_1 \tag{14}$$

where $y_1=[\psi_1\ Q_a]^T$ and Q_a is the volumetric flow through S_{a2}.

The analysis for Case 2 is similar to Case 1. Considering the effective mass of φ_2 as $m_{\varphi_2}=\rho\frac{A_2}{3}\frac{h_2^2+4\ell_0^2}{h_2}$, then the air velicities and kinetic energy in Ω_2 are given by

[1] As a consequence of irrotational assumption, the air velocity in the sagittal axis is neglected.

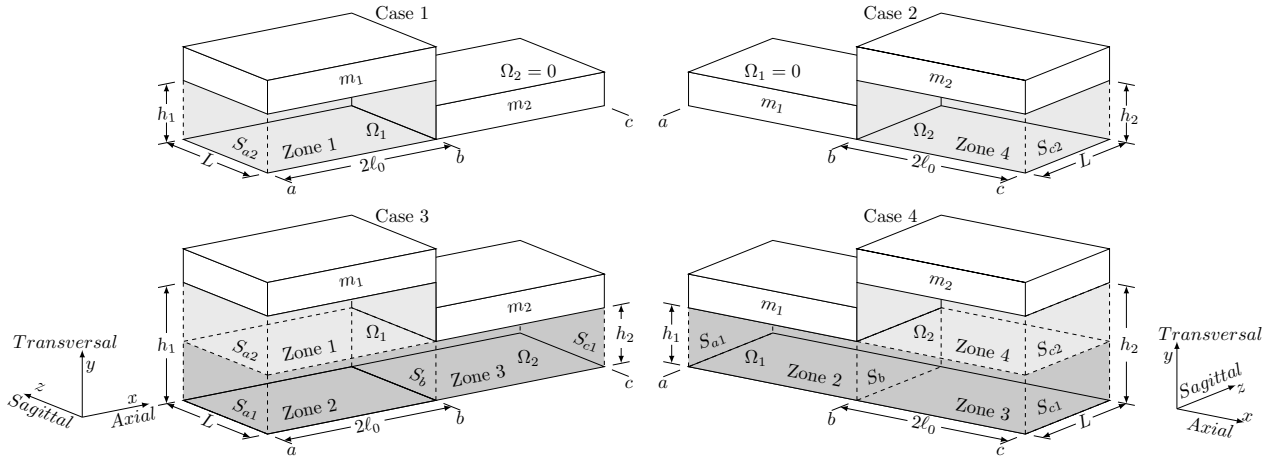

Fig. 2. Glottis configurations

$$\vartheta_2 = -\frac{\psi_2}{h_2}(\ell_0 + x) \qquad \varphi_2 = \frac{\psi_2}{h_2} y \tag{15}$$

$$\mathcal{E}_2 = \frac{1}{2} C_{\varphi_2} \pi_{\varphi_2}^2 \tag{16}$$

Following the same procedure presented for Case 1, the energy balance in Ω_2 is given by

$$\begin{aligned}\dot{\mathcal{E}}_2 &= -A_{c2}\vartheta_{2c2}P_c - \mathcal{D}_c - \psi_2 F_2 \\ &= \psi_2 \left(A_2 P_c - \frac{2\ell_0}{h_2} g_2 \frac{\partial \mathcal{E}_2}{\partial \pi_{\varphi_2}} s_{c2} - F_2 \right)\end{aligned} \tag{17}$$

where $P_c = \langle p \rangle_{S_{a2}}$, $g_2 = \frac{\rho}{2} A_2 \vartheta_{2c2}$ and s_{c2} is equal to 1 when $\vartheta_{2c2} > 0$ and 0 otherwise.

From (17) and the time derivative of (16) the PH model for Case 2 is given by

$$\dot{x}_2 = \begin{bmatrix} 0 & 1 \\ -1 & -\frac{2\ell_0}{h_2} g_2 s_{c2} \end{bmatrix} \nabla \mathcal{E}_2 + \begin{bmatrix} 0 & 0 \\ -1 & A_2 \end{bmatrix} \begin{bmatrix} F_2 \\ P_c \end{bmatrix} \tag{18}$$

$$y_2 = \begin{bmatrix} 0 & -1 \\ 0 & A_2 \end{bmatrix} \nabla \mathcal{E}_2 \tag{19}$$

where $x_2 = [h_2 \ \pi_{\varphi_2}]^T$, $y_2 = [\psi_2 \ -Q_c]^T$ and Q_c is the volumetric flow through S_{c2}.

2.2 Model for Case 3 and Case 4

For Case 3 the boundary conditions for the airflow in Ω_1 are given by $\vartheta_1|_{y>h_b} = 0$, $\varphi_1|_{y=h_1} = \psi_1$, $\varphi_1|_{y=h_b} = \psi_1 h_b/h_1$ and $\varphi_1|_{y=0} = 0$ where $h_b = \min(h_1, h_2)$. Then solving (1) we obtain

$$\vartheta_1 = \begin{cases} \psi_1 \dfrac{\ell_0 - x}{h_1}, & y > h_b \\ \theta_1 - \psi_1 \dfrac{x}{h_1}, & y \le h_b \end{cases}, \qquad \varphi_1 = \psi_1 \frac{y}{h_1} \tag{20}$$

where θ_1 is the average axial velocity in Zone 2 (see Figure 2). The total kinetic energy in Ω_1 is given by

$$\mathcal{E}_1 = \int_{\Omega_1} \frac{\rho}{2} |\mathbf{v}_1|^2 d\Omega_1 = \frac{1}{2} m_{\vartheta_1} \theta_1^2 + \frac{1}{2} m_{\varphi_1} \psi_1^2 \tag{21}$$

where $m_{\varphi_1} = \frac{\rho A_1}{3} \frac{h_1^3 + \ell_0^2(4h_1 - 3h_b)}{h_1^2}$ and $m_{\vartheta_1} = \rho A_1 h_b$.

Remark 1. Note that (20)-(21) correspond to the velocities and kinetic energy in Ω_1 for Case 3 when $h_b = h_2$, and for Case 4 when $h_b = h_1$, *i.e*, the model can be used for both cases.

Remark 2. Moreover, when $h_b = h_2$ and h_2 tends to 0, the velocities and kinetic energy in (20)-(21) reduce to the velocities and energy obtaining for Case 1 in (2) and (4).

The energy balance in Ω_1 for case 3, is given by

$$\begin{aligned}\dot{\mathcal{E}}_1 &= A_{a1}\vartheta_{1a2}P_a + A_{a2}\vartheta_{1a2}P_a - \mathcal{D}_a \\ &\quad - \psi_1 F_1 - A_b \vartheta_{1b} P_b\end{aligned} \tag{22}$$

where we have considered that the pressure P_a in S_{a1} and S_{a2} is uniform and where $A_{a1} = A_b = L h_b$ and $A_{a2} = L(h_1 - h_b)$.

The analysis for Case 4 is similar to Case 3. The air velocities and kinetic energy in Ω_2 are given by

$$\vartheta_2 = \begin{cases} -\psi_2 \dfrac{\ell_0 + x}{h_2}, & y > h_b \\ \theta_2 - \psi_2 \dfrac{x}{h_2}, & y \le h_b \end{cases}, \qquad \varphi_2 = \psi_2 \frac{y}{h_2} \tag{23}$$

$$\mathcal{E}_2 = \frac{1}{2} m_{\vartheta_2} \theta_2^2 + \frac{1}{2} m_{\varphi_2} \psi_2^2 \tag{24}$$

where θ_2 is the average axial velocity in Zone 3 (see Figure 2), $m_{\varphi_2} = \frac{\rho A_2}{3} \frac{h_2^3 + \ell_0^2(4h_2 - 3h_b)}{h_2^2}$ and $m_{\vartheta_2} = \rho A_2 h_b$.

Remark 3. As notice in Remark 1 for Ω_1 in Case 3, (23)-(24) describe the velocities and energy in Ω_2 for both Case 3 and Case 4.

Remark 4. Additionally, when $h_b = h_1$ and h_1 tends to 0, the velocities and energy of Case 2 are obtained.

The energy balance for Ω_2 is given by

$$\begin{aligned}\dot{\mathcal{E}}_2 &= -A_{c1}\vartheta_{2c1}P_c + A_{c2}\vartheta_{2c2}P_c - \mathcal{D}_c \\ &\quad - \psi_2 F_2 + A_b \vartheta_{2b} P_b\end{aligned} \tag{25}$$

Rewriting (21) and (24) as a function of the corresponding momenta and considering $\dot{h}_b = \psi_1 s_b + \psi_2 \bar{s}_b$ where $s_b = 1$ for $h_1 < h_2$ and $s_b = 0$ otherwise, and $\bar{s}_b = (1 - s_b)$, then the total energy of fluid in $\Omega = \{\Omega_1, \Omega_2\}$, is given by

$$\mathcal{E}_F = \sum_i K_{fi} = \sum_i C_{\vartheta_i} \pi_{\vartheta_i}^2 + C_{\varphi_i} \pi_{\varphi_i}^2 \tag{26}$$

$$\begin{aligned}\dot{\mathcal{E}}_F &= \theta_1 \dot{\pi}_{\vartheta_1} + \theta_2 \dot{\pi}_{\vartheta_2} + \psi_1 \left(\dot{\pi}_{\varphi_1} + \frac{\partial \mathcal{E}_F}{\partial h_1} + \frac{\partial \mathcal{E}_F}{\partial h_b} s_b \right) \\ &\quad + \psi_2 \left(\dot{\pi}_{\varphi_2} + \frac{\partial \mathcal{E}_F}{\partial h_2} + \frac{\partial \mathcal{E}_F}{\partial h_b} \bar{s}_b \right)\end{aligned} \tag{27}$$

where K_{fi} is the kinetic energy of the airflow in $\Omega_i, i \in \{1,2\}$.

On the other hand, the power dissipation through the transversal surfaces in points a and c are given by

$$\mathcal{D}_a = -\kappa_d A_{a1}\frac{\rho}{2}\vartheta_{1a1}^3 s_{a1} - \kappa_d A_{a2}\frac{\rho}{2}\vartheta_{1a2}^3 s_{a2} \tag{28}$$

$$\mathcal{D}_c = \kappa_d A_{c1}\frac{\rho}{2}\vartheta_{2c1}^3 s_{c1} + \kappa_d A_{c2}\frac{\rho}{2}\vartheta_{2c2}^3 s_{c2} \tag{29}$$

The forces associated to the dynamic pressure are given by $\kappa_d A_{a1}\frac{\rho}{2}\vartheta_{1a1}^2 = -g_1\vartheta_{1a2}$, $\kappa_d A_{a2}\frac{\rho}{2}\vartheta_{1a2}^2 = -g_2\vartheta_{1a2}$, $\kappa_d A_{c1}\frac{\rho}{2}\vartheta_{2c1}^2 = g_3\vartheta_{2c1}$ and $\kappa_d A_{c2}\frac{\rho}{2}\vartheta_{2c2}^2 = -g_4\vartheta_{2c2}$, with $g_1 = -\kappa_d\frac{\rho}{2}A_{a1}\vartheta_{1a2}$, $g_2 = -\kappa_d\rho A_{a2}\vartheta_{1a2}$, $g_3 = \kappa_d\frac{\rho}{2}A_{c1}\vartheta_{2c1}$ and $g_4 = \kappa_d\rho A_{c2}\vartheta_{2c2}$.

Remark 5. Note that when s_{a1}, s_{a2}, s_{c1} and s_{c2}, are active (i.e., equal to 1), the energy dissipation factors g_1, g_2, g_3 and g_4 are positive.

To model the power transfer between Ω_1 and Ω_2 through the point b, we consider that the power balance on S_b is $\mathcal{X}_{S_b} = 0$,*i.e*, there is no loss of energy in S_b, and by mass conservation law, $\vartheta_{1b} = \vartheta_{2b}$. Then $\mathcal{X}_{S_b}$ can be written as

$$\begin{aligned}\mathcal{X}_{S_b} &= \kappa_x A_b\left(\frac{\rho}{2}\vartheta_{1b}^3 - \frac{\rho}{2}\vartheta_{2b}^3\right)\\ &= \kappa_x A_b\left(\vartheta_{1b}\frac{\rho}{2}\vartheta_{2b}^2 - \vartheta_{2b}\frac{\rho}{2}\vartheta_{1b}^2\right) = 0\end{aligned} \tag{30}$$

where κ_x is an exchange energy factor (κ_d and κ_x, in (9) and (30) respectively, are adjusted such that the model satisfies the mass conservation law). Additionally, the dynamic pressures in S_b can be rewritten as $\kappa_x A_b\frac{\rho}{2}\vartheta_{1b}^2 = f_1\vartheta_{1b}$ and $\kappa_x A_b\frac{\rho}{2}\vartheta_{2b}^2 = f_1\vartheta_{2b}$ where $f_1 = \kappa_x\frac{\rho}{2}A_b\vartheta_{1b} = \kappa_x\frac{\rho}{2}A_b\vartheta_{2b}$. Then the energy balance for Case 3 and Case 4 is given by

$$\dot{\mathcal{E}}_F = \sum_i \dot{\mathcal{E}}_i - \sum_k \mathcal{D}_k - \mathcal{X}_{S_b} \tag{31}$$

where $i = \{1,2\}$ and $k = \{a,c\}$.

Finally, substituting (22), (25) and (28)-(30) in (31), and equating to (27), we obtain the following PH model of the fluid ($\mathcal{M}_F$)

$$\dot{x}_F = \begin{bmatrix}\mathbf{0}_{3\times3} & J_2\\ -J_2^T & \begin{pmatrix}-R_1 & J_1\\ -J_1^T & -R_2\end{pmatrix}\end{bmatrix}\nabla\mathcal{E}_F + \begin{bmatrix}\mathbf{0}_{3\times4}\\ G_1\end{bmatrix}u_F \tag{32}$$

$$y_F = \begin{bmatrix}\mathbf{0}_{4\times3} & G_1^T\end{bmatrix}\nabla\mathcal{E}_F \tag{33}$$

where $x_F = [h_1\ h_2\ h_b\ \pi_{\vartheta_1}\ \pi_{\varphi_1}\ \pi_{\vartheta_2}\ \pi_{\varphi_2}]^T$ are state variables, $u_F = [P_a\ P_c\ F_1\ F_2]^T$, $y_F = [Q_a\ -Q_c\ \psi_1\ \psi_2]^T$ and

$$J_1 = \begin{bmatrix}-f_1 & -\frac{\ell_0}{h_2}f_1\\ \frac{\ell_0}{h_1}f_1 & \frac{\ell_0^2}{h_1h_2}f_1\end{bmatrix} \qquad J_2 = \begin{bmatrix}0&1&0&0\\0&0&0&1\\0&s_b&0&\bar{s}_b\end{bmatrix}$$

$$R_1 = \begin{bmatrix}g_1s_{a1} & \frac{\ell_0}{h_1}g_1s_{a1}\\ \frac{\ell_0}{h_1}g_1s_{a1} & \frac{\ell_0^2}{h_1^2}g_5\end{bmatrix} \qquad R_2 = \begin{bmatrix}g_3s_{c1} & -\frac{\ell_0}{h_2}g_3s_{c1}\\ -\frac{\ell_0}{h_2}g_3s_{c1} & \frac{\ell_0^2}{h_2^2}g_6\end{bmatrix}$$

$$G_1 = \begin{bmatrix}A_b & 0 & 0 & 0\\ \frac{A_1}{2}\frac{2h_1-h_b}{h_1} & 0 & -1 & 0\\ 0 & -A_b & 0 & 0\\ 0 & \frac{A_1}{2}\frac{2h_2-h_b}{h_2} & 0 & -1\end{bmatrix}$$

where $g_5 = g_1s_{a1} + 2g_2s_{a2}$ and $g_6 = g_3s_{c1} + 2g_4s_{c2}$. Note that from Remarks 1-4, this model is valid for the four cases represented in Figure 2.

3. MASS-SPRING-DAMPER MODEL

In this section, we expand the PH model of Encina et al. (2015) to obtain a full description of the dynamics of the body-cover model (Story and Titze, 1995). We use the auxiliary position variables h_{ic} to model the elastic collision of each mass. The state variables of this model are given by $x_S = [h_1\ h_{1c}\ h_2\ h_{2c}\ h_3\ \pi_1\ \pi_2\ \pi_3]^T$, where h_2, h_1 and h_3 are the displacement of upper, lower and body masses respectively, $h_{ic's}$ and $\pi_{i's}$ are the collision displacement and momenta of the each mass (see Figure 1).

Defining $\Delta h_i = h_i - h_{i0}$, where h_{i0} is the equilibrium position of the mass m_i, the total energy of the mass-spring-damper system, is given by

$$\mathcal{E}_S = \sum_j U_j + \sum_k K_k \tag{34}$$

where $j = \{1, 1c, 2, 2c, 3, c\}$, $k = \{1,2,3\}$ and

$$\begin{aligned}U_1 &= \frac{k_1}{2}(\Delta h_1 - \Delta h_3)^2 + \frac{k_1\eta_1}{4}(\Delta h_1 - \Delta h_3)^4\\ U_2 &= \frac{k_2}{2}(\Delta h_2 - \Delta h_3)^2 + \frac{k_2\eta_2}{4}(\Delta h_2 - \Delta h_3)^4\\ U_3 &= \frac{k_3}{2}(\Delta h_3)^2 + \frac{k_3\eta_3}{4}(\Delta h_3)^4\end{aligned}$$

are the stored energy functions for the lateral springs of each mass, where k_j and η_j are the linear and nonlinear coefficients for the corresponding springs. Similarly

$$\begin{aligned}U_{1c} &= \frac{k_{1c}}{2}h_{1c}^2 + \frac{k_{1c}\eta_{1c}}{4}h_{1c}^4\\ U_{2c} &= \frac{k_{2c}}{2}h_{2c}^2 + \frac{k_{2c}\eta_{2c}}{4}h_{2c}^4\\ U_c &= \frac{k_c}{2}(\Delta h_2 - \Delta h_1)^2\end{aligned}$$

are the stored energy functions for the collision and coupling springs, and

$$K_1 = \frac{1}{2}\frac{\pi_1^2}{m_1}, \qquad K_2 = \frac{1}{2}\frac{\pi_2^2}{m_2}, \qquad K_3 = \frac{1}{2}\frac{\pi_3^2}{m_3}$$

are the stored (kinetic) energy functions for the masses. As a result, the mass-spring-damper differential equations of (Story and Titze, 1995) can be rewritten as the following PH model ($\mathcal{M}_S$)

$$\dot{x}_S = \begin{bmatrix}\mathbf{0}_{5\times5} & J_3\\ -J_3^T & -R_3\end{bmatrix}\nabla\mathcal{E}_S + \begin{bmatrix}\mathbf{0}_{5\times2}\\ G_2\end{bmatrix}u_S \tag{35}$$

$$y_s = \begin{bmatrix}\mathbf{0}_{2\times5} & G_2^T\end{bmatrix}\nabla\mathcal{E}_S \tag{36}$$

where $y_S = [\psi_1\ \psi_2]$, $u_S = [F_1\ F_2]$ and

$$J_3 = \begin{bmatrix}1&0&0\\ s_1&0&0\\ 0&1&0\\ 0&s_2&0\\ 0&0&1\end{bmatrix} \qquad R_3 = \begin{bmatrix}d_1&0&-d_1\\ 0&d_2&-d_2\\ -d_1&-d_2&r_{s1}\end{bmatrix} \qquad G_2 = \begin{bmatrix}0&1\\1&0\\0&0\end{bmatrix}$$

and the switch signals s_1 and s_2 change from 0 (free movement mode) to 1 (collision mode) when m_1 and m_2 collide, respectively, d_j are the dampers coefficients and $r_{s1} = d_1 + d_2 + d_3$.

4. INTERCONNECTION

In this section, we interconnect the fluid and structure PH models, $\mathcal{M}_F$ and $\mathcal{M}_S$. We use the interconnection approach presented in Lopes and Hélie (2016). Considering that $h_i \in \mathcal{M}_F$ are equal to the corresponding $h_i \in \mathcal{M}_S$, then $\frac{\partial \mathcal{E}_F}{\partial \pi_{\varphi_i}} = \frac{\partial \mathcal{E}_S}{\partial \pi_i}$, i.e,

$$C_{\varphi_i}\pi_{\varphi_i} = \frac{\pi_i}{m_i} \tag{37}$$

However, the boundary conditions used in Section 2 to solve (1), produce that $\psi_i \to 0$ when $h_i \to 0$, i.e, a non-elastic collision. For a more realistic modeling of the vocal folds behavior, elastic collisions are required. For this purpose, we define a threshold value ϵ, such that, in Ω_i, we disconnect the fluid dynamics from the structure when $h_i < \epsilon$, leading to a switching port-Hamiltonian model (Gerritsen et al., 2002; Van der Schaft and Camlibel, 2009; Van der Schaft and Jeltsema, 2014). Considering that the switching variables s_{ϵ_i} are equal to 1 when $h_i \geq \epsilon$ and 0 otherwise, we construct the total energy function of the fluid-structure system as [2]

$$H = \mathcal{E}_S + \mathcal{E}_F(s_{\epsilon_i}) = \sum_j U_j + \sum_k K_k + \sum_i s_{\epsilon_i} K_{fi} \tag{38}$$

Now defining the total vertical momentum in Ω_i as [3]

$$\pi_{yi} = \pi_i + s_{\epsilon_i}\pi_{\varphi_i} \tag{39}$$

from (37) and (39), we can write the kinetic energy associated to π_{yi} as

$$\begin{aligned} K_{yi} &= K_i + s_{\epsilon_i} K_{fi} \\ &= \frac{1}{2}\left(\frac{1}{m_i} - \frac{s_{\epsilon_i}}{m_i(1+m_i C_{\varphi_i})}\right)\pi_{yi}^2 + \frac{1}{2} s_{\epsilon_i} C_{\vartheta_i} \pi_{\vartheta_i}^2 \end{aligned}$$

Then we can rewrite the total energy as

$$H = \sum_j U_j + \sum_i K_{yi} + K_3 \tag{40}$$

From the models $\mathcal{M}_F$ and $\mathcal{M}_S$, we obtain that

$$\dot{\pi}_{yi} = \dot{\pi}_i + s_{\epsilon_1}\dot{\pi}_{\varphi_i} \tag{41}$$

Using (37), (39), and $s_{\epsilon_i}^2 = s_{\epsilon_i}$, we can rewrite the dynamics in (41) as a function of ∇H. Finally, defining the state variables $x = [h_1\ h_{1c}\ h_2\ h_{2c}\ h_3\ h_b\ \pi_{\vartheta_1}\ \pi_{y1}\ \pi_{\vartheta_2}\ \pi_{y2}\ \pi_3]^T$, the following port-Hamiltonian Fluid-Structure model ($\mathcal{M}_{FS}$) is obtained

$$\dot{x} = \begin{bmatrix} \mathbf{0}_{6\times 6} & \mathcal{J}_2 \\ -\mathcal{J}_2^T & \mathcal{J}_1 - \mathcal{R}_1 \end{bmatrix} \nabla H + \begin{bmatrix} \mathbf{0}_{6\times 2} \\ \mathcal{G} \end{bmatrix} u \tag{42}$$

$$y = \begin{bmatrix} \mathbf{0}_{2\times 6} & \mathcal{G}^T \end{bmatrix} \nabla H \tag{43}$$

where $u = [P_a\ P_c]^T$, $y = [Q_a\ -Q_c]$ and

$$\mathcal{J}_1 = \begin{bmatrix} 0 & 0 & -l_1 & -l_2 & 0 \\ 0 & 0 & l_3 & l_4 & 0 \\ l_1 & -l_3 & 0 & 0 & 0 \\ l_2 & -l_4 & 0 & 0 & 0 \\ 0 & 0 & 0 & 0 & 0 \end{bmatrix} \quad \mathcal{J}_2 = \begin{bmatrix} 0 & 1 & 0 & 0 & 0 \\ 0 & s_1 & 0 & 0 & 0 \\ 0 & 0 & 0 & 1 & 0 \\ 0 & 0 & 0 & s_2 & 0 \\ 0 & 0 & 0 & 0 & 1 \\ 0 & s_{\epsilon_{1b}} & 0 & s_{\epsilon_{2b}} & 0 \end{bmatrix}$$

[2] Recall that K_{fi} is the fluid kinetic energy in Ω_i

[3] Recall that π_{φ_i} is the fluid vertical momentum in Ω_i

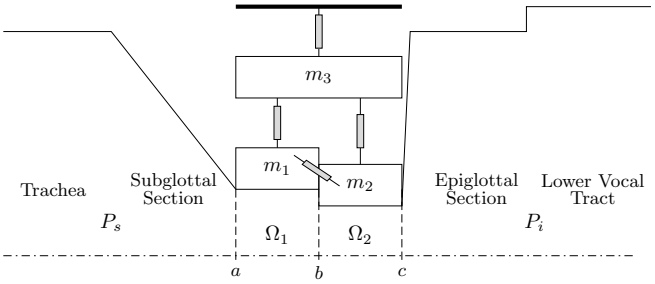

Fig. 3. Glottis structure considered to analyze the pressure behavior

$$\mathcal{R}_1 = \begin{bmatrix} r_1 & r_2 & 0 & 0 & 0 \\ r_2 & r_5 & 0 & 0 & -d_1 \\ 0 & 0 & r_3 & r_4 & 0 \\ 0 & 0 & r_4 & r_6 & -d_2 \\ 0 & -d_1 & 0 & -d_2 & r_{s1} \end{bmatrix}$$

$$\mathcal{G} = \begin{bmatrix} A_b & s_{\epsilon_1}\frac{A_1}{2}\frac{2h_1 - h_b}{h_1} & 0 & 0 & 0 \\ 0 & 0 & -A_b & s_{\epsilon_2}\frac{A_2}{2}\frac{2h_2 - h_b}{h_2} & 0 \end{bmatrix}^T$$

where $l_1 = s_{\epsilon_1}s_{\epsilon_2}f_1$, $l_2 = s_{\epsilon_1}s_{\epsilon_2}\frac{\ell_0 f_1}{h_2}$, $l_3 = s_{\epsilon_1}s_{\epsilon_2}\frac{\ell_0 f_1}{h_1}$, $l_4 = s_{\epsilon_1}s_{\epsilon_2}\frac{\ell_0^2 f_1}{h_1 h_2}$, $s_{\epsilon_{1b}} = s_{\epsilon_1}s_b$, $s_{\epsilon_{2b}} = s_{\epsilon_2}\bar{s_b}$, $r_1 = s_{a1}s_{\epsilon_1}g_1$, $r_2 = s_{a1}s_{\epsilon_1}\frac{\ell_0 g_1}{h_1}$, $r_3 = s_{c1}s_{\epsilon_2}g_3$, $r_4 = s_{c1}s_{\epsilon_2}\frac{\ell_0 g_3}{h_2}$, $r_5 = d_1 + s_{\epsilon_1}\frac{\ell_0^2 g_5}{h_1^2}$ and $r_6 = d_2 + s_{\epsilon_2}\frac{\ell_0^2 g_6}{h_2^2}$.

5. SIMULATIONS

For the simulations we use Matlab/Simulink with ODE15s solver. We use the parameters in Table II, case C in Story and Titze (1995) . For the fluid, we use the air density $\rho = 1.43\times 10^{-3}\text{gr/cm}^3$, $\epsilon = 1.8\times 10^{-3}\text{cm}$, $\kappa_d = 10.5$, $\kappa_x = 2.5$. To obtain P_a and P_c, we analyze the pressure behavior in the glottis, including the subglottal and epiglottal sections, as shown in Figure 3. We use the pressure description in Ishizaka and Flanagan (1972) and Story and Titze (1995) for subglottal and epiglottal sections respectively, *i.e.*,

$$P_a = P_s - \frac{\rho}{2}Q_a^2\left(\frac{k_s}{A_a^2} - \frac{1}{A_s^2}\right) \tag{44}$$

$$P_c = P_i - \frac{\rho}{2}Q_c^2\frac{k_e}{A_c^2} \tag{45}$$

where $k_s = 1 + \lambda_s$, $\lambda_s = 0.36$ is a loss factor and k_e is the epiglottal pressure recovery coefficient. The pressure solution in Ω_1 and Ω_2 is obtained from the motion equation of fluids (Bird et al., 2014).

Equating the pressures in P_b from Ω_1 and Ω_2, solving for Q_b^2, and substituting in (44) and (45) (considering that $Q_a = Q_b + A_1\psi_1$ and $Q_c = Q_b - A_2\psi_2$), we obtain (Mora, 2017)

$$P_a = P_s + \frac{w_1}{w_b}(P_s - P_i) + \frac{\rho w_2}{2w_b}(2Q_a A_1\psi_1 - A_1^2\psi_1^2) \tag{46}$$

$$P_c = P_i - \frac{w_3}{w_b}(P_s - P_i) - \frac{\rho w_4}{2w_b}(2Q_c A_2\psi_2 + A_2^2\psi_2^2) \tag{47}$$

where $w_b = (1-k_e)A_b^{-2} - A_s^{-2} - (1-k_s)A_a^{-2}$, $w_1 = (A_s^{-2} - k_s A_a^{-2}$, $w_2 = (A_s^{-2} - k_s A_a^{-2})(1-k_e)A_c^{-2}$, $w_3 = k_e A_c^{-2}$ and $w_4 = k_e A_c^{-2}\left((1-k_e)(A_c^{-2} + A_b^{-2}) - A_s^{-2} - (1-k_s)A_a^{-2}\right)$.

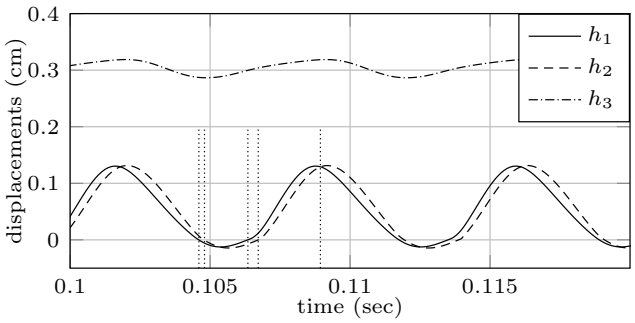

Fig. 4. Displacement of each mass using (46)

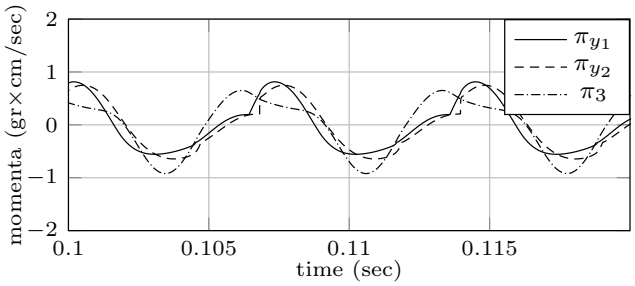

Fig. 5. Momenta associated to the vertical movements

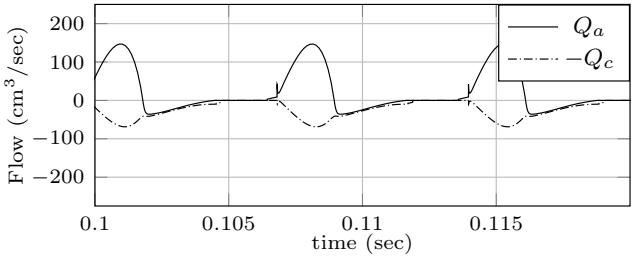

Fig. 6. Outputs of the port-Hamiltonian model

Considering a subglottal and supraglottal areas of 5cm^2, the movement of each mass, using (46)-(47), is shown in Figure 4. It can be noticed that the masses exhibit oscillations with a fundamental frequency of 140 Hz. Additionally, the transition instants (dotted lines) between the four cases studied in Section 2 can be observed.

Figure 5 shows the momenta associated to vertical movements Finally, the volumetric flows in points a and c are shown in Figure 6. Note that, compared to the Story and Titze (1995) model, the $\mathcal{M}_{FS}$ model allows to distinguish the airflows in the lower and upper parts of the glottis (Q_a and Q_c respectively) and, also, to obtain negative flow values.

6. CONCLUSION

In this paper we presented a port-Hamiltonian model of the vocal folds as an example of a fluid-structure interconnection system. We extended the model by Encina et al. (2015) including a port-Hamiltonian representation of the fluid dynamics based on the approach proposed by Lopes and Hélie (2016). The simulations obtained are in corresponding with the movement of the vocal folds. The structure model and the fluid model were used to obtain a port-Hamiltonian model for the whole system, based on the signals in common.An interconnection of both subsystems based on ports requires an alternative way to describe the fluid model and is currently under development.

REFERENCES

Bird, R.B., Stewart, W.E., Lightfoot, E.N., and Klingenberg, D.J. (2014). *Introductory Transport Phenomena*. John Wiley & Sons, United States of America.

Cardoso-Ribeiro, F.L., Matignon, D., and Pommier-Budinger, V. (2017). A port-Hamiltonian model of liquid sloshing in moving containers and application to a fluid-structure system. *Journal of Fluids and Structures*, 69(December 2016), 402–427. doi: 10.1016/j.jfluidstructs.2016.12.007.

Encina, M., Yuz, J., Zañartu, M., and Galindo, G. (2015). Vocal fold modeling through the port-hamiltonian systems approach. In *IEEE Multiconference on Systems and Control - MSC 2015*. Sydney, Australia. doi: 10.1109/CCA.2015.7320832.

Gerritsen, K.M., Van der Schaft, A.J., and Heemels, W.P.M.H. (2002). On Switched Hamiltonian Systems. In D.S. Gilliam and J. Rosenthal (eds.), *Fifteenth International Symposium on Mathematical Theory of Networks and Systems (MTNS 2002)*, 1–21. Indiana, USA.

Hager, W.H. (2010). Losses in Flow. In *Wastewater Hydraulics*, 17–54. Springer Berlin Heidelberg, second edition. doi:10.1007/978-3-642-11383-3_2.

Hamamoto, M., Ohta, Y., Hara, K., and Hisada, T. (2005). Design of flexible wing for flapping flight by fluid-structure interaction analysis. In *Proceedings of the 2005 IEEE International Conference on Robotics and Automation*, 2253–2258. doi: 10.1109/ROBOT.2005.1570448.

Ishizaka, K. and Flanagan, J.L. (1972). Synthesis of Voiced Sounds From a Two Mass Model of the Vocal Cords. *Bell System Technical Journal*, 51(6), 1233–1268. doi: 10.1002/j.1538-7305.1972.tb02651.x.

Lopes, N. and Hélie, T. (2016). Energy balanced model of a jet interacting with a brass playe's lip. *Acta Acustica United with Acustica*, 102.

Mora, L. (2017). Analysis of the glottal pressures. Technical report, UTFSM. URL `http://altair.elo.utfsm.cl/show.php?id=4571`.

Story, B.H. and Titze, I.R. (1995). Voice simulation with a body cover model of the vocal folds. *The Journal of the Acoustical Society of America*, 97(2), 1249–1260. doi:10.1121/1.412234.

Van der Schaft, A.J. and Camlibel, M.K. (2009). A state transfer principle for switching port-Hamiltonian systems. *Proceedings of the IEEE Conference on Decision and Control*, 45–50. doi:10.1109/CDC.2009.5400785.

Van der Schaft, A. and Jeltsema, D. (2014). Port-Hamiltonian Systems Theory: An Introductory Overview. *Foundations and Trends® in Systems and Control*, 1(2), 173–378. doi:10.1561/2600000002.